Entrainment to the CIECAM02 and CIELAB colour appearance models in the human cortex

Andrew Thwaites[1,2*], Cai Wingfield[1,3], Eric Wieser[4], Andrew Soltan[5], William D. Marslen-Wilson[1,2], Ian Nimmo-Smith[2]

[1] Department of Psychology, University of Cambridge, Cambridge, UK
[2] MRC Cognition and Brain Sciences Unit, Cambridge, UK
[3] Department of Psychology, University of Lancaster, Lancaster, UK
[4] Department of Engineering, University of Cambridge, Cambridge, UK
[5] School of Clinical Medicine, University of Cambridge, Cambridge, UK

*Corresponding author. Department of Psychology, Downing Site, University of Cambridge, Cambridge, CB2 3EB, United Kingdom
E-mail address: acgt2@cam.ac.uk

Keywords: CIECAM02, CIELAB, magnetoencephalography, colour perception, model expression, entrainment

Abbreviations: V1, primary visual cortex; EMEG, electro- and magneto-encephalographic; KID, Kymata identifier; CIECAM02, the CIE (2002) colour appearance model; CIELAB, the CIEL*A*B (1976) colour space; ERG, electroretinographic; LGN, lateral geniculate nucleus

Abstract

In human visual processing, information from the visual field passes through numerous transformations before perceptual attributes such as colour are derived. The sequence of transforms involved in constructing perceptions of colour can be approximated by colour appearance models such as the CIE (2002) Colour Appearance Model, abbreviated as CIECAM02. In this study, we test the plausibility of CIECAM02 as a model of colour processing by looking for evidence of its cortical entrainment. The CIECAM02 model predicts that colour is split into two opposing chromatic components, red-green and cyan-yellow (termed CIECAM02-a and CIECAM02-b respectively), and an achromatic component (termed CIECAM02-A). Entrainment of cortical activity to the outputs of these components was estimated using measurements of electro- and magnetoencephalographic (EMEG) activity, recorded while healthy subjects watched videos of dots changing colour. We find entrainment to chromatic component CIECAM02-a at approximately 35 ms latency bilaterally in occipital lobe regions, and entrainment to achromatic component CIECAM02-A at approximately 75 ms latency, also bilaterally in occipital regions. For comparison, transforms from a less physiologically plausible model (CIELAB) were also tested, with no significant entrainment found.

(180 words)

1 Introduction

As information travels through the human visual system, it is subjected to a variety of transformations. First, the cornea and the lens alter the spectral content of incoming light (Bone and Sparrock, 1971). This filtered light then strikes the retina, where photoreceptor cones with different spectral absorption rates activate at different wavelengths (Stockman et al., 1999; Stockman and Sharpe, 2000). The excitation from these photoreceptors (L-, M- and S-cones) is integrated through sets of neuronal cells in the inner retinal layer, which quantifies the colour information into three opponent channels. The first of these channels quantifies achromatic information[1], and is comprised of the aggregate L and M excitation information (sometimes written 'L+M')[2]. The remaining two channels quantify chromatic information: the 'L-M' cone opponent channel (comprised of the difference between the incoming L and M signals) is the basis of the red-green channel of colour vision, while 'S-[L+M]' (in which the S-cone signals are antagonistic to those from L- and M-cones) is the basis of the cyan-yellow channel (Lee and Silveira, 2016). Each channel projects from the retina into the lateral geniculate nucleus (LGN); the L+M channel projecting predominantly to the magnocellular layer; the L-M channel to the parvocellular layer, and the S-[L+M] channel to the koniocellular layer. These channels are thus also known as the MC-, PC- and KC-pathways. From the LGN, the pathways project into an area of the visual cortex known as V1, where colour information is passed to the extra striate cortex. The precise nature of the transformations involved in the processing of colour from V1 onwards is less clear (Conway, Chatterjee, et al., 2010; Shapley and Hawken, 2011; Johnson and Mullen, 2016).

One of the most effective ways to ascertain the sequence of transformations that visual information undergoes has been to examine whether hypothesised transformations are 'tracked' by neuronal or cortical activity, a phenomenon known as entrainment (Ding, et al., 2014; Ding and Simon, 2014). For example, the L+M and L-M transformations are found to be entrained in both electroretinogram (ERG) and intracellular in vitro recordings on inner retinal layers (ERG: Kremers and Link, 2008; Kremers et al, 2010; Parry et al, 2012; see Kremers et al (2016) for overview; intracellular recordings: Dacey et al, 1996).

The ability to model sequences of transformations is therefore an important precursor to testing for evidence of entrainment. While the transformations that have taken place at the retina are relatively straightforward (with visual information having passed through a relatively small number of neurons), hypothesising the sequence of transformations at V1 or beyond is more challenging. The most comprehensive of these later sequences are the 'colour appearance' models, which characterise the transformations hypothesised to occur in the perception of colour. The formulation of

[1] The achromatic response is sometimes referred to as 'luminance'.

[2] The extent to which S-cone information contributes to the achromatic channel is a question of some debate (Ripamonti et al, 2009).

these models has historically been informed both by retinal physiology and the behavioural responses of human observers to colour stimuli (Luo and Hunt 1998).

In the current study, we test four hypothesised transformations for cortical entrainment, comprising the achromatic and red-green transformations from each of two colour appearance models, CIELAB and CIECAM02. CIELAB was developed during the 1970s and served for many years as the Joint ISO/CIE Standard for colour appearance; its successor, CIECAM02, was released in 2002 and included the addition of more complex features which aimed to model the visual system and observed behavioural responses to colour perception more accurately (Moroney et al., 2002). While the use of CIELAB is prevalent, being widely used in the domains of technology and engineering, it is less physiologically plausible than its successor, and can be considered a naïve baseline model against which CIECAM02 can be compared. The CIECAM02 achromatic transformation is referred to as CIECAM02-A, while the red-green chromatic transformation is referred to as CIECAM02-a. Their CIELAB counterparts are denoted CIELAB-L and CIELAB-A respectively.

As noted by Parry et al. (2012), both achromaticity and chromaticity are known to be computed in parallel, and as a result it is possible to observe entrainment of the two transformations simultaneously using a single stimulus. In the current study, we use an established procedure (Thwaites et al., 2015; 2016; 2017) to search for evidence of entrainment to CIECAM02 and CIELAB in the neural activity of regions of the cortex (striate, extra striate, and regions beyond), measured by electroencephalography (EEG) and magnetoencephalography (MEG). Specifically, we aim to determine (1) whether entrainment to achromaticity and chromaticity occurs for either model, and if so: (2) the latencies and (3) location of this entrainment.

Evidence of entrainment of both achromatic and red-green colour opponency has already been identified in the visual-occipital cortex. EEG and MEG studies have identified entrainment directly (achromatic: Regan, 1966; Herrmann, 2001; chromatic: Cheng et al., 2001; Nishifuji et al., 2006) and when the signal has been convolved with an impulse response, estimated using evoked spread spectrum analysis (Lalor et al., 2006, VanRullen and Macdonald, 2012). Evidence of entrainment of achromatic and red-green colour opponency to blood oxygenation levels (BOLD), measured through functional Magnetic Resonance Imaging (fMRI), has also been reported (achromaticity: Kwong, et al (1992); Ogawa et al., 1992; Wandell and Winawer, 2011 for historical overview; red-green response: McKeefry and Zeki (1997), Hadjikhani et al., 1998). The current study is the first to test for evidence of entrainment to the widely adopted specific colour appearance models CIECAM02 and CIELAB, as well as being the first reporting precise latencies of that entrainment.

In addition to the static graphic presentation of results in this paper, a dynamic, interactive representation of this study's results can be viewed on the online Kymata

Atlas (http://kymata.org). For easy reference, each hypothesised transformation in this paper (referred to as a 'function' in Kymata) is assigned a *Kymata ID* (KID).

2 Methods

2.1 Defining candidate models

A suitable model is one that takes a set of time-varying signals as input (in this case the visual field) and produces a time-varying signal as output (the predication of neural activity). The model must be characterized by a function *f*, taking the form:

$$f(x_1,x_2,x_3,...,x_t) = (y_1,y_2,y_3,...,y_t), \quad \text{(eq 1)}$$

where input $(x_1,...,x_t)$ and output $(y_1,...,y_t)$ are both time-courses of length t, and where f is bounded by a set of formal requirements (Davis et al., 1994) and the additional requirement that y_i cannot be dependent on any x_k where $k>i$. This latter requirement excludes non-causal functions from the outset, such that each output y_i can depend only on the input history $(x_1, ..., x_i)$. In the current work, we test models that are a special case, where y_i is dependent on x_i alone (although we consider the opportunity for testing models that make use of historical inputs in the discussion).

In the following section, we specify four candidate models based on different hypothesised transforms of visual data.

2.2 The CIECAM02 models

Colour appearance models seek to capture the perception of colour under diverse viewing conditions (Fairchild, 2013). The foundation of these models lies in colour opponency (Hering, 1878), in which there are two opposing colour dimensions: red-green and cyan-yellow. Together with an achromatic response value, these allow the full range of colours to be encoded (see Judd, 1951; Wandell, 1995 for overview).

In this study we consider a contemporary colour appearance model based on opponent colour, the CIE (2002) Colour Appearance Model (Moroney et al., 2002), abbreviated as CIECAM02. A simplified schematic is shown in Fig 1C. First, the stimulus colour is represented as L(t), M(t), S(t) tristimulus values, in the LMS-space of Li et al.

(2002). These are then transformed to the L′M′S′-space (Hunt-Pointer-Estevez space) of Hunt and Pointer (1985)[3]:

$$\boldsymbol{L'M'S'}(t) = \begin{bmatrix} L'(t) \\ M'(t) \\ S'(t) \end{bmatrix} = \begin{bmatrix} 0.38971 & 0.68898 & -0.07868 \\ -0.22981 & 1.18340 & 0.04641 \\ 0.00000 & 0.00000 & 1.00000 \end{bmatrix} * \begin{bmatrix} L(t) \\ M(t) \\ S(t) \end{bmatrix} \quad \text{(eq. 2)}$$

where $L(t)$, $M(t)$, and $S(t)$ are the viewing-condition-adapted tristimulus values in LMS-space of the stimulus at time t.

These L′, M′ and S′ values then undergo non-linear response compression based on a generalised Michaelis-Menten equation:

$$L'_a(t) = \frac{400(F_L L'(t)/100)^{0.42}}{27.13+(F_L L'(t)/100)^{0.42}} + 0.1 \quad \text{(eq. 3)}$$

where F_L is a luminance-level adaptation factor specific to the viewing parameters (see Fairchild (2013) for discussion). Values of $M'_a(t)$ and $S'_a(t)$ can be calculated from $M'(t)$ and $S'(t)$ in a similar manner, substituting L' with M' or S'.

The complete pipeline of transforms for CIECAM02, and their justifications, can be found in Moroney et al.'s CIECAM02 schema.

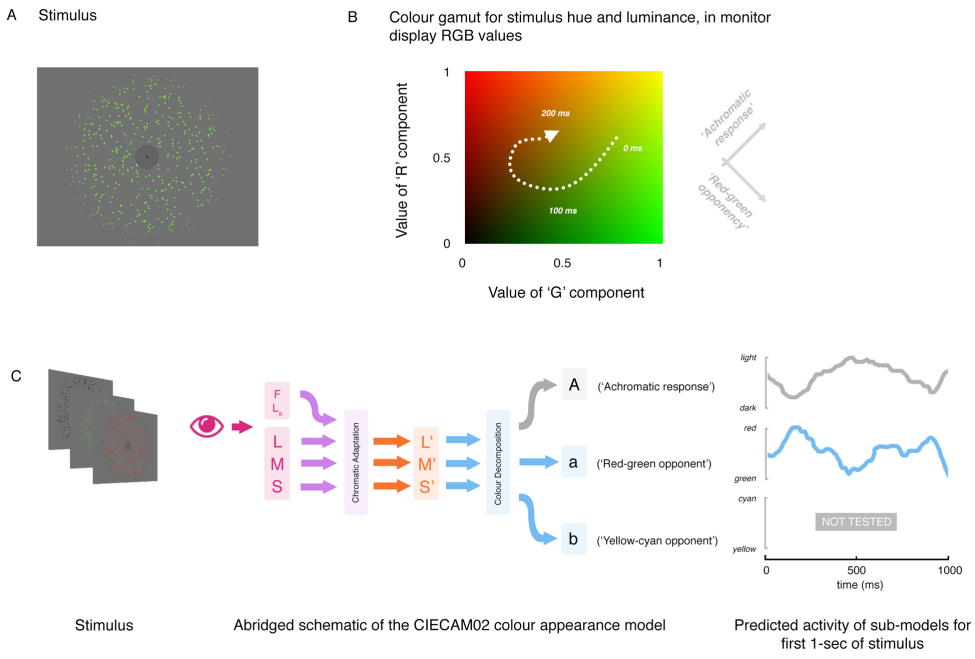

[3] LMS- and L′M′S′-space are also referred to as RGB- and R′G′B′-space by some authors, including Moroney et al., Li et al., and Hunt and Pointer.

Fig 1. Example of the stimulus, and model predictions. A. The stimulus consisted of coloured dots on a grey background, with a fixation cross in the centre. B. The colour of the dots varied over time, and was generated by taking a random trajectory through a red-green-black-yellow colour gamut. C. Abridged schematic of the CIECAM02 colour appearance model, together with the predicted electrophysiological activation of the *achromatic response* (CIECAM02-A) and *red-green* (CIECAM02-a) model components for the first second of the stimulus.

2.2.1 CIECAM02-A (KID: Q5D5M)

The function CIECAM02-A models the achromatic response to a stimulus in the visual field. It takes the form:

$$\text{CIECAM02\_}A(t) = [2L_a(t) + M'_a(t) + (1/20)S'_a(t) - 0.305]N_{bb} \qquad \text{(eq. 4)}$$

where $L'_a(t)$, $M'_a(t)$, and $S'_a(t)$ are the compressed $L'(t)$, $M'(t)$ and $S'(t)$ values of the stimulus at time t and N_{bb} is the chromatic induction factor specific to the viewing condition parameters. The value of this variable over the first 1 second of the stimulus is shown in Fig 1C.

2.2.2 CIECAM02-a (KID: URKWX)

The function CIECAM02-A models the red-green colour opponent value of a stimulus in the visual field. It takes the form:

$$\text{CIECAM02\_}a(t) = 2L'_a(t) - 12M'_a(t)/11 + S'_a(t)/11 \qquad \text{(eq. 5)}$$

where $L'_a(t)$, $M'_a(t)$, and $S'_a(t)$ are the compressed $L'(t)$, $M'(t)$ and $S'(t)$ values of the stimulus at time t. The value of this variable over the first 1 second of the stimulus is shown in Fig 1C.

2.3 The CIELAB models

The CIELAB colour appearance model (also known as CIEL*A*B*) is a precursor to CIECAM02. Like CIECAM02, it models colour opponency, but is comparatively naïve and ignores physiologically plausible features of colour processing such as the application of chromatic adaptation to a space closer to cone fundamental space (Fairchild, 2013). Despite its relative simplicity, CIELAB is a widely used colour space employed in cameras and visual processing equipment, and was adopted as a Joint ISO/CIE Standard (ISO 11664-4:2008(E)/CIE S 014-4/E:2007). In this study we use it as a naïve comparator to the more physiologically plausible CIECAM02.

2.3.1 CIELAB-L (KID: 68RA6)

The function CIELAB-L models the achromatic response to a stimulus in the visual field. Its inputs are X(t), Y(t), and Z(t) tristimulus values, defined in the CIE 1931 XYZ colour space (ISO 11664-1:2007). The model takes the following form:

$$CIELAB\_L(t) = 116\left(\begin{cases} if\ {}^{Y(t)}/_{Y_{ref}(t)} > 0.008856\ then\ \left({}^{Y(t)}/_{Y_{ref}(t)}\right)^{1/3} \\ else\ 7.787 * \left({}^{Y(t)}/_{Y_{ref}(t)}\right) + {}^{16}/_{116} \end{cases}\right)$$

where Y(t) is the average tristimulus value over the visual field, and Y_{ref}(t) is the normalised tristimulus value of the reference field (in this experiment Y_{ref}(t) was kept constant at a value of 100).

2.3.1 CIELAB-A (KID: UYBPJ)

The function CIELAB-A models the red-green colour opponent value of a stimulus in the visual field. It takes the following form:

$$CIELAB\_A(t) = 500\left(\begin{cases} if\ {}^{X(t)}/_{X_{ref}(t)} > 0.008856\ then\ \left({}^{X(t)}/_{X_{ref}(t)}\right)^{1/3} \\ else\ 7.787 * \left({}^{X(t)}/_{X_{ref}(t)}\right) + {}^{16}/_{116} \end{cases}\right.$$
$$\left. - \begin{cases} if\ {}^{Y(t)}/_{Y_{ref(t)}} > 0.008856\ then\ \left({}^{Y(t)}/_{Y_{ref(t)}}\right)^{1/3} \\ else\ 7.787 * \left({}^{Y(t)}/_{Y_{ref(t)}}\right) + {}^{16}/_{116} \end{cases}\right)$$

where X(t) and Y(t) are the average tristimulus values of the visual field, and X_{ref}(t) and Y_{ref}(t) are the tristimulus values of the reference field (in this experiment we used constant values X_{ref}(t) = 95.04 and Y_{ref}(t) = 100).

2.4. The analysis procedure

The reconstructed distributed source current of the cortex is specified as the current of 10,242 cortical regions (sources), spaced uniformly over the cortex. The testing procedure involves examining each of these sources, looking for evidence that the current predicted by a model is similar to the current observed (Fig. 2A). This procedure is repeated at 5 ms intervals (Fig. 2B) across a range of time-lags ($-200 < l < 800$ ms), covering the range of plausible latencies (0 to 800 ms) and a short, pre-stimulation range (–200 to 0 ms) during which we expect to see no entrainment. This produces a statistical parametric map that changes over time as the lag is varied, revealing the changes in similarity of a given model's predicted behaviour with observed behaviour over the cortical surface. Evidence of a model's similarity

between its predicated behaviour and measured cortical activity is expressed as a p-value, which is generated through the match-mismatch technique described in Thwaites et al. (2015), where evidence for similarity is described as significant if the p-value falls below a pre-defined threshold, α*. We refer to the observation of significant matches at a specific lag and location as 'model expression'.

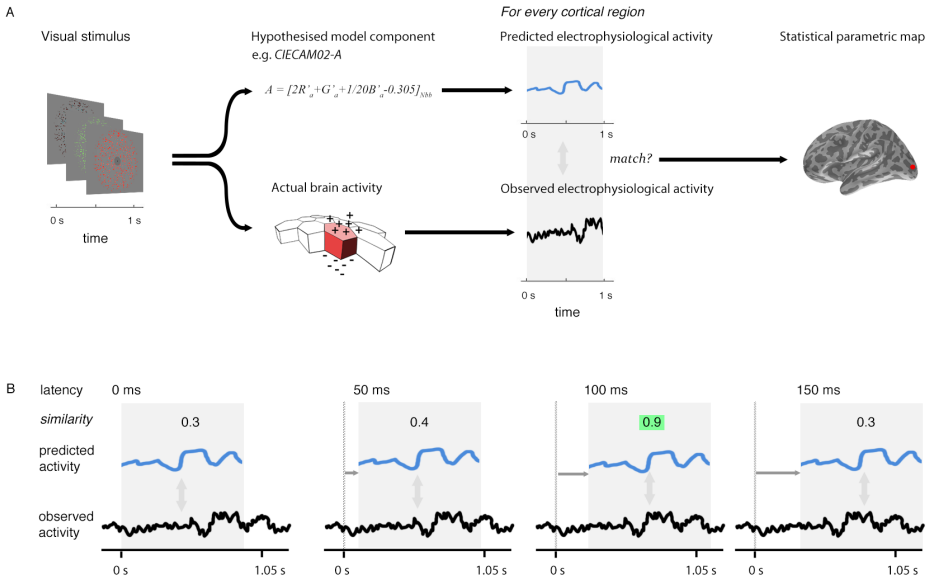

Fig 2. Technique overview. First (A), the electrophysiological activity of the brain in response to a given stimulus (measured using EMEG) is matched to the pattern of neural activity predicted by the model being evaluated. Predicted and observed activity are tested for similarity and the resulting Statistical Parametric Map (SPM) displays the regions (vertices) where the match is statistically significant. Second (B), this procedure is repeated at different lags (illustrated here from 0-150 ms) between the onset of the observed neural activity and the onset of the predicted output. We record the lag at which the similarity is greatest (highlighted). This produces an SPM that changes over time.

Setting α* so that it accurately reflects what we know about the data being tested can be difficult. In the current study, some of the measurements used in the tests would be dependent on other measurements (because of spatial and temporal similarities between neighbouring sources and lags). However, it is very difficult, if not impossible, to get accurate estimations of, for instance, the spatial dependencies between sources. In the present study, rather than accept assumptions about the dependencies that are hard to justify, we assumed that the data at each source and lag were independent (a 'worst case' scenario), prompting us to use a Bonferroni-type correction. As a result, the reader should be aware that the type II error rate is likely to be high, making the reported results very conservative.

We used the formula for the familywise false alarm rate from Thwaites et al. (2015) to generate an α^* of approximately 3×10^{-13}; p-values greater than this are deemed to be not significant.

The results are presented as *expression plots*, which show the latency at which each of the 10,242 sources per hemisphere best matched the output of the tested model (marked as a 'stem'). On the y-axis is the evidence of the match at this latency: if any of the sources have evidence, at their best latency, indicated by a p-value lower than α^*, they are deemed significant matches and the stems are coloured red, blue, pink and green depending on the model.

The expression plots also allow us to chart which models are most likely to be entrained at a particular source through a model selection procedure, using p-values as a proxy for model likelihood. By default, the expression plot displays only the best model (i.e. the one with the lowest p-value) for a source. It is important to note that this model selection procedure does not indicate that any one model is *significantly* better than another for some source. It indicates only that one model fits the data to a somewhat higher degree than another, even if this evidence may not differ strongly between models. We take this approach as we are only interested in the trend of which models explain the activity best in each source, and to disambiguate between models which may be correlated over time.

2.5. MEG and EEG Methods and Materials

2.5.1 Experiment design

Participants: 15 right-handed participants (7 men, mean age = 24 years, range=18-30) were recruited. All gave informed consent and were paid for their participation. The study was approved by the Peterborough and Fenland Ethical Committee (UK), and the study was carried out in accordance with the Code of Ethics of the World Medical Association (Declaration of Helsinki).

Stimuli: A pattern of randomly placed dots with a grey mask in the surrounds and centre. The centre also contained a black fixation cross (Fig. 1A). The colour and horizontal movement of these dots fluctuated pseudo-randomly. The stimulus lasted 6 minutes and 40 seconds, allowing it to be split later in the analysis procedure into 400 segments of length 1000 ms. 10 seconds of stimulus were added to the beginning and end of the stimulus to avoid the sudden appearance and disappearance of the stimulus during the first and last trial.

The colour of the dots during the experiment was controlled by independently fluctuating the R and G base components of the monitor display pixels between 0.3 and 1. The B base component remained at zero throughout the experiment. Although values for the monitors R and G were explicitly manipulated, the axes of interest are at roughly 45 degrees to this: the red-green opponency dimension (i.e., the ratio of red

to green in the colour's hue), and achromaticity dimension (the luminance of the resulting colour value). These fluctuations were pseudo-periodic, with frequencies ranging between 4 and 40Hz (see Fig 1B).

Although the B base component remained constant during the stimulus, it does not follow that the cyan-yellow opponency response (not tested during the study) likewise remained constant. Indeed, this would not be possible without choosing a measure of cyan-yellow opponency beforehand: CIECAM02 and CIELAB define the cyan-yellow chromaticity dimensions in different manners, and they cannot both be maintained at a single value simultaneously. Thus, the choice to fix B = 0 was made to simplify the stimulus definition and not to control for the B-component in the signal.

2.5.2. Procedure

Each participant received one practice stimulus lasting 20 seconds. The continuous 6 minute and 40 second stimulus was played 4 times to the participant, with instructions to fixate on the cross in the middle of the screen. After each presentation, the participant could rest, playing the next presentation when ready, using a button box. Presentation of stimuli was controlled with Matlab, using the Psychophysics Toolbox extensions (Brainard, 1997; Pelli, 1997; Kleiner et al., 2007). The stimuli were presented on a Panasonic PT-D7700 DLP projector, with the central wavelengths of the red, green and blue base components being 610, 550 and 472 nm respectively (measured using a Coherent Inc. spectroscope), while the CIE xyY coordinates of these components were (0.64, 0.33, 0.22), (0.26, 0.61, 0.71) and (0.16, 0.07, 0.72) respectively (measured using an Admesy Brontes tristimulus colorimeter). The energies of these components were Gamma-corrected for the projector.

To keep participants alert during the experiment, the subjects listened passively to an audio podcast (a BBC radio talk-show) while watching the stimuli.

2.5.3 Modelling the predicted CIECAM02 and CIELAB entrainment responses

The changing hue and luminance of the colours were displayed on the projector in monitor RGB format (as described in section 2.5.1). However, the CIECAM02 and CIELAB models both require the momentary XYZ tristimulus values (and their accompanying viewing parameters) as input. An Admesy Brontes tristimulus colorimeter was used to measure the momentary XYZ values of the projector stimulus over time, giving an accurate measurement of these values during the projection of the stimulus. These XYZ values (together with measurement or estimation of the accompanying viewing parameters), were then used to calculate the CIELAB and CIECAM02 responses, using the equations given in section 2.2 and 2.3.

2.5.4. EMEG recording

Continuous MEG data were recorded using a 306 channel VectorView system (Elekta-Neuromag, Helsinki, Finland) containing 102 identical sensor triplets (two orthogonal planar gradiometers and one magnetometer) in a hemispherical array situated in a light magnetically-shielded room. The position of the head relative to the sensor array was monitored continuously by four Head-Position Indicator (HPI) coils attached to the scalp. Simultaneous EEG was recorded from 70 Ag-AgCl electrodes placed in an elastic cap (EASYCAP GmbH, Herrsching-Breitbrunn, Germany) according to the 10/20 system, using a nose electrode as reference. Vertical and horizontal EOG were also recorded. All data were sampled at 1 kHz with a band-pass filter from 0.03-330 Hz. A 3-D digitizer (Fastrak Polhemus Inc., Colchester, VA) recorded the locations of the EEG electrodes, the HPI coils and approximately 50-100 'headpoints' along the scalp, relative to three anatomical fiducials (the nasion and left and right pre-auricular points).

2.5.5. Data pre-processing

Static MEG bad channels were detected and excluded from subsequent analyses (MaxFilter version 2, Elekta-Neuromag, Stockholm, Sweden). Compensation for head movements (measured by HPI coils every 200 ms) and a temporal extension of the signal–space separation technique (Taulu et al*.,* 2005) were applied to the MEG data. Static EEG bad channels were visually detected and removed from the analysis (MNE version 2.7., Martinos Center for Biomedical Imaging, Boston, Massachusetts). The EEG data were re-referenced to the average over all channels. The continuous data were low-pass filtered to 100 Hz (zero-phase shift, overlap-add, FIR filtering). The recording was split into 400 epochs of 1000 ms duration. Each epoch included the 200 ms from before the epoch onset and 800 ms after the epoch finished (taken from the epoch previous and subsequent) to allow for the testing of different latencies. Epochs in which the EEG or EOG exceeded 200 μV, or in which the value on any gradiometer channel exceeded 2000 fT/m, were rejected from both EEG and MEG datasets (between 5% and 15%, depending on the participant). Epochs that were not rejected were averaged over all four stimulus repetitions.

2.5.6. Source Reconstruction

The location of the cortical current sources was estimated using minimum-norm estimation (MNE; Hämäläinen and Ilmoniemi, 1994), neuro-anatomically constrained by MRI images obtained using a GRAPPA 3D MPRAGE sequence (TR=2250 ms; TE=2.99 ms; flip-angle=9 degrees; acceleration factor=2) on a 3T Tim Trio (Siemens, Erlangen, Germany) with 1 mm isotropic voxels. For each participant a representation

of their cerebral cortex was constructed using FreeSurfer (Freesurfer 5.3, Martinos Center for Biomedical Imaging, Boston, Massachusetts) from their individual MR images. The forward model was calculated with a three-layer Boundary Element Model using the outer surface of the scalp and the outer and inner surfaces of the skull identified in the structural MRI. Anatomically-constrained source activation reconstructions at the cortical surface were created by combining MRI, MEG, and EEG data. The MNE representations were down-sampled to 10,242 vertices per hemisphere, roughly 3mm apart, to improve computational efficiency. Representations of individual subjects were aligned using a spherical morphing technique (Fischl et al., 1999). Source activations for each trial were averaged over participants. We employed a loose-orientation constraint (0.2) to improve the spatial accuracy of localization. Sensitivity to neural sources was improved by calculating a noise covariance matrix based on a 1 second pre-stimulus period. Reflecting the reduced sensitivity of MEG sensors for deeper cortical activity (Hauk et al., 2011), sources located on the cortical medial wall and in subcortical regions were not included in the analyses reported here.

The entrainment testing procedure (section 2.4) was performed on these participant-average source reconstructions.

2.5.7. Visualization

The cortical slices in Fig 3. use the visualization software MRIcron (Georgia State Center for Advanced Brain Imaging, Atlanta, Georgia) with results mapped to the high-resolution colin27 brain (Schmahmann et al., 2000).

3. Results

3.1 CIECAM02 model

3.1.1 CIECAM02-A component ('the achromatic response')

The regions where expression for the CIECAM02-A model was the most significant of the models tested — and below the α* threshold — were located bilaterally at 75 ms (Fig. 3B), centred in regions in the occipital lobe. An interactive representation of this model (and all models tested in this paper) can be viewed using the Kymata Atlas (2016).

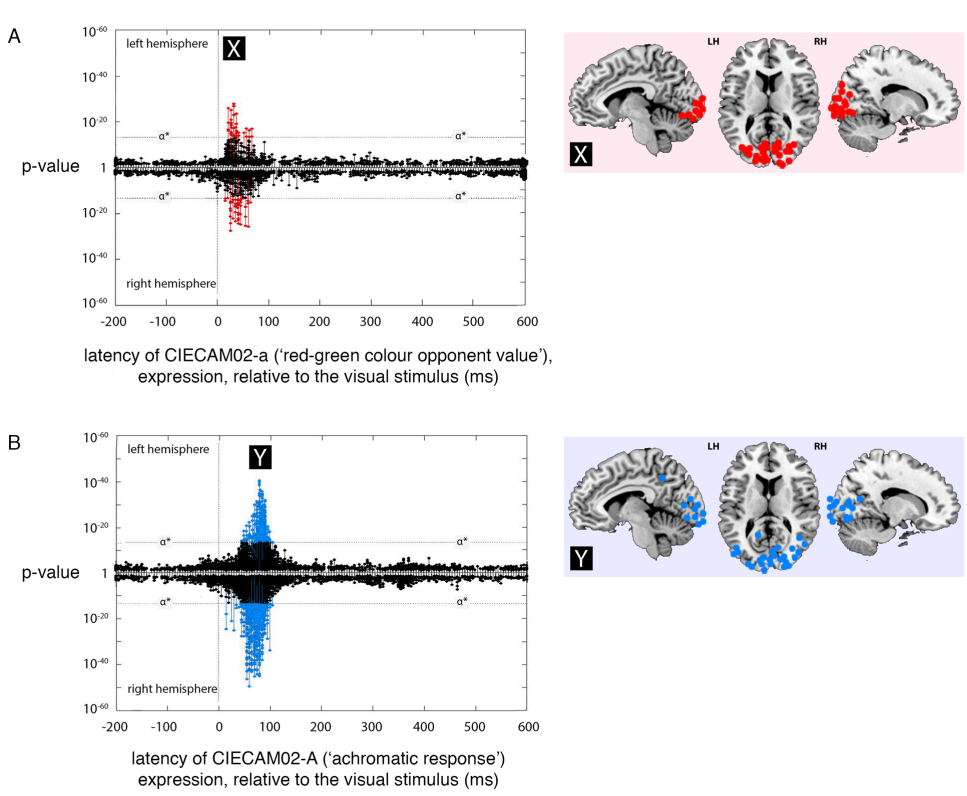

Fig 3. Expression plots for CIECAMO2-A and CIECAMO2-a from the CIECAM02 colour appearance model. A) Plot for the expression for the CIECAMO2-a model across processing lags from -200 to +600 ms, relative to the visual environment. Results for the left and right hemispheres are plotted separately, mirror-wise across the mid-line. The minimum p-values at a given source, over all latencies, are marked as 'stems'. Stems at or 'above' the stipulated value ($p \simeq 3\times10^{-13}$) indicate significant expression of the CIECAMO2-a (red) at that source. **B)** Plot for the expression for the CIECAMO2-A model (blue). The peaks for both models' significant expression are marked X (at 35 ms, CIECAMO2-a) and Y (75 ms, CIECAMO2-A). The cortical locations of significant sources are indicated on the coronal and sagittal slices to right of the plots. These plot implements model selection (see **section 2.4**) so that each source only appears once in 3A, 3B, 4A and 4B.

The locations (namely ventral, posterior parietal, calcarine sulcus and occipital lobe regions) are approximate in all cases, as a consequence of the error introduced by the point-spread function inherent in EMEG source localization (see discussion). This spatial ambiguity means it is not possible to narrow these locations to specific visual areas, beyond noting that the entrainment is centred around the occipital pole (V1).

3.1.2 CIECAM02-a component ('red-green opponent colour dimension')

The regions where expression for the CIECAM02-a model was the most significant of the two models tested, and passed the α* threshold, were located bilaterally at 35 ms (Fig. 3A). Like CIECAM02-A, these regions were centred in ventral, posterior parietal, calcarine sulcus and occipital lobe.

3.1.2 CIELAB-L and CIELAB-a components

No significant expression was found for either CIELAB-L or CIELAB-A, at any latency (Fig. 4).

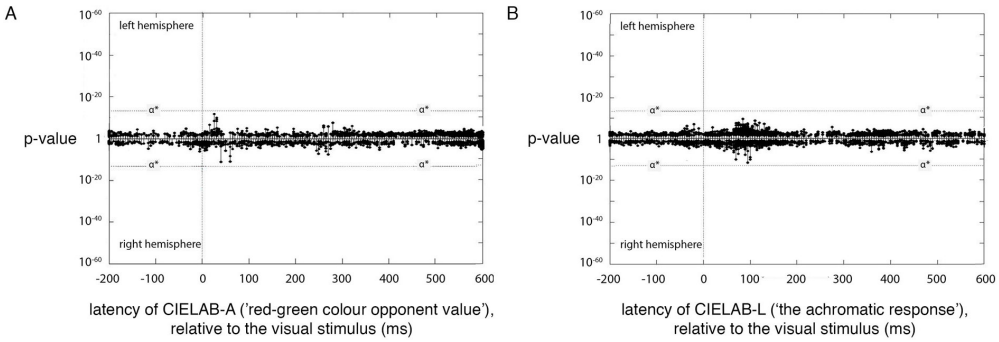

Fig 4. Expression plots for CIELAB-A and CIELAB-L from the CIELAB colour appearance model. A) Plot for the expression for the CIELAB-A across lags from -200 to +600 ms, relative to the visual environment. **B)** Plot for the expression for the CIELAB-L. Neither show significant entrainment at any latency.

4 Discussion

As noted in the introduction, entrainment to the transformations for both achromaticity and red-green opponency are found in the output of the inner retinal layer as inputs to the MC- and PC-pathway respectively. The question in this study was whether entrainment to CIECAM02 models of these features can be found in the cortical activity at the point where these pathways enter the cortex. Our results indicate that this is the case: evidence of significant entrainment for both CIECAM02-A and CIECAM02-a is centred bilaterally in the polar occipital cortex, the region of visual area V1, and the region where the afferent pathways project into the cortex. Although focused on the poles, there is significant entrainment of the output for both transformations in ventral, posterior parietal, and calcarine sulcus areas. The reader should be cautious about narrowing down the location of the entrainment to either component more narrowly. The inherent insolvability of the inverse problem during EMEG source reconstruction (Grave de Peralta-Menendez et al., 1996; Grave de Peralta-Menendez and Gonzalez-Andino, 1998) means that substantial 'point spread' of localization data may be present. Improvements in source reconstruction (through

the gathering of more data or improved inverse techniques) may reduce this error in the future.

These findings are consistent with previous reports which locate entrainment to chromaticity and achromaticity in the human visual-occipital cortex, in both dendritic current (Regan, 1966; Herrmann, 2001; Cheng et al., 2001; Nishifuji et al., 2006) and blood oxygenation levels (Kwong, et al (1992); Ogawa et al., 1992; McKeefry and Zeki (1997), Hadjikhani et al., 1998). However, the current study is the first to test for evidence of entrainment to CIECAM02 and CIELAB. Historically, the most informative entrainment studies have been those in which the outputs of explicit physiological mechanisms (modelled as mathematical transforms) are tested: a preeminent example is Derrington and colleagues, who, in their landmark study (Derrington et al, 1984), tested the entrainment of cell responses in the PC- and MC-pathway to the modulation of opponency channels modelled on the physiologically-based 'MBDKL' colour space (MacLeod and Boynton, 1978; Derrington et al, 1984). This ability to link the predictions of such models with measured physiological responses is a powerful tool in assessing the plausibility of the model themselves. The current study, which tests the plausibility of two rival models that aim to characterise both perceptual and physiological properties (CIECAM02, and CIELAB) against each other, emphasises this potential: the results demonstrate significant entrainment to CIECAM02 achromaticity and red-green opponency (Fig 3), compared with no significance for their CIELAB counterparts (Fig 4). The insignificance of CIELAB is no doubt due to the fact that, compared with CIECAM02, it is comparatively naïve; CIELAB ignores physiologically plausible features of colour processing such as chromatic adaptation to a space akin to that of the cone fundamentals, features which are modelled by CIECAM02. As a result, the entrainment pattern of CIECAM02 is likely to match the observed electrophysiological activity better than that of that of CIELAB, leading to the analysis procedure giving the former a higher plausibility.

The most striking difference between the CIECAM02 achromatic and red-green response components is the latency difference: CIECAM02-a is entrained at 35 ms, while CIECAM02-A is entrained at 75ms, a full 40 ms later (Fig 3; Fig 5). This result is consistent with previous findings showing the achromatic response lagging the chromatic response (e.g. Walraven and Leebeek, 1964, see Kommanapalli et al (2014) for overview). Kommanapalli et al. (2014) argue that this difference may be due to retinal physiology: L- and M- cones that serve as inputs to chromatic (parvocellular) ganglion cells appear to provide their respective inputs at the same latency (Smith et al, 1992); by contrast, L- and M- cones inputs to achromatic (magnocellular) ganglion cells appear to provide their respective inputs at different latencies (with M- lagging L- between 5 and 35 ms), and it is plausible that this delay of the M- input relative to the L- input results in the entire achromatic pathway being delayed with respect to its chromatic counterpart. It is worth noting that a delay of achromatic information relative to chromatic information does not contradict evidence that red-green colour opponency responses appear to be lost at high temporal frequencies (Ives, 1912), a

result that has traditionally been taken as evidence that the MC-pathway is able to process achromatic signals 'more rapidly' than the red-green PC-pathway. The fact the achromatic pathway is able to encode higher frequencies than the red-green pathway does not necessitate it arriving at the cortex before red-green information.

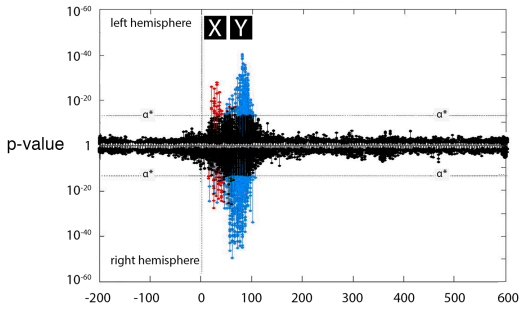

Fig 5. Expression distributions for CIECAM02-a and CIECAM02-A superimposed on a single plot. Figs 3A (**CIECAM02-a, red**) and 3B (**CIECAM02-A, blue**) are superimposed to show CIECAM02-A lagging CIECAM02-a by 40 ms. As in Fig 3, the peaks for both models' significant expression are marked X (at 35 ms, CIECAMO2-a) and Y (75 ms, CIECAMO2-A).

If this latency mismatch is indeed a result of delay caused by retinal physiology, what repercussions might this have on downstream visual processing? The output of colour opponency processing is thought to feed into processes such as edge and relief detection (Hansen and Gegenfurtner, 2009; Kingdom, 2003), and a mismatch in latency must affect such processes, at least for rapidly moving stimuli. Either the two channels are integrated with the delay still present, or the chromatic representation would need to be delayed in order to correct the difference. If the latter, we might expect to observe a secondary spike of entrainment to CIECAM02-a at 75 ms, demonstrating that CIECAM02-a had become re-synchronised. But such an observation would not be necessary for such an account to hold – both CIECAM02-a and CIECAM02-A may have further transforms applied to them before being resynchronised. Given that the present study is not designed to be sensitive to such models, it suggests a need for future research.

Overall, the results of this study support the view that visual information from the L- and M-cones integrate into a single red-green opponent channel in the manner modelled by CIECAM02-a, which exhibits entrainment at 35 ms delay in the occipital lobe region of the cortex. In parallel to this, visual information from the L- and M-cones combine into an achromatic channel in the manner modelled by CIECAM02-A, exhibiting entrainment at 75 ms delay in the occipital lobe region (Fig 6.)

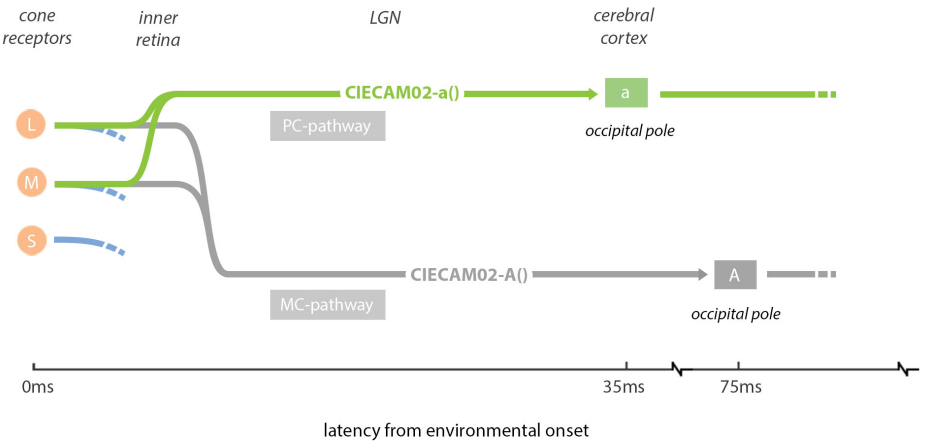

Fig 6. Implied pathway of red-green colour opponent and achromatic response information. The interpretation of the pathways suggested by the findings of this study. Information from the visual field enters the nervous system as L, M and S values, from which L and M is combined into the CIECAM02-a model component, exhibiting entrainment at 35 ms in the occipital lobe region of the cortex. In parallel, L- and M-cone information is combined into the CIECAM02-A model component, exhibiting in entrainment at 75 ms in the occipital lobe region of the cortex. In the model, both components also receive minor inputs from S cones, but these contributions have been left out for clarity. The incomplete blue pathways leaving L, M, S are the assumed inputs to the cyan-yellow KC-pathway (not tested in this study).

It should be emphasized that this characterisation — based on plausibilities of the models tested in this study — must be seen as a simplification of the full picture of chromatic and achromatic transforms taking place between the retina and V1. While single-cell recordings in macaque and rhesus monkeys confirm that the retina, LGN and V1 all contain cells which are selective to chromatic or achromatic information (e.g. retina: Gouras, 1968; De Monasterio and Gouras, 1975; LGN: Derrington et al, 1984; Levitt et al, 2001; V1: Johnson et al, 2001; Conway, 2001), such cells, both in the retina and LGN, have also been shown to carry other properties of the stimulus, for example the ratio of stimulus's centre/surround in the cells' receptive field (De Monasterio and Schein, 1980; Wiesel and Hubel, 1966). Indeed, it appears colour-opponency cells are tuned to a range of properties: in V1 these include spatial frequency, orientation and more complex hue spaces (Leventhal, et al, 1995; Johnson et al, 2008; Wachtler et al, 2003), as well as cells that respond to both luminance and colour (Johnson et al, 2001; Johnson et al, 2004; Thorell, et al 1984), and there are indications of tuning to properties such as orientation as early as LGN MC- and PC-cells (Xu et al, 2000). This indicates a picture where the steps in visual processing leading to colour perception are complex combination of transforms that take place over the retina-LGN-V1 pathway.

The findings reported in this study open a number of avenues for further work. First, repeating the above study using electroretinography may help identify the latency at which various chromatic components leave the retina; this would, in turn, narrow down the latency window between which these components travelled from the retina to V1. Testing cortical entrainment to the cyan-yellow colour opponent response (as estimated by CIECAM02-b) is a second reasonable extension to this work; the KC-pathway is less studied that the pathways tested above and its delay in latency relative to the PC- and MC-pathways is unknown. It would also be beneficial to test further components of the CIECAM02 model beyond the three central colour pathways, as well as rival colour opponency and luminance models (e.g. Kunkel and Reinhard, 2009). The CIECAM02 model does not, for instance, take into account historical values of visual input, and so does not model the fact that red-green entrainment is reported to break down for higher frequencies (Ives, 1912).

4.1 Overview

The results from this study suggest that the CIECAM02-a transform of the visual field occurs before a latency of 35 ms, with entrainment to the output of this transform occurring at 35 ms latency bilaterally in occipital lobe regions. In parallel to this, the CIECAM02-A transform also takes place, with entrainment occurring at 75 ms, also in the occipital lobe regions. By comparison, no entrainment was found to the relatively physiologically naive CIELAB-L and CIELAB-A components. The locations of the significant entrainment are only approximate due to the inherent error in source estimation of EMEG data and more work is needed in improving the accuracy of these reconstructions in order to improve the certainty of these locations.

5. Data statement

The data used in this study (including stimuli, EMEG recordings and pre-processed data) can be found at https://kymata.org/datasets, available under a CCBY licence.

6. Acknowledgements

This work was supported by an ERC Advanced Grant (Neurolex) to WMW and by MRC Cognition and Brain Sciences Unit (CBU) funding to WMW (U.1055.04.002.00001.01). Computing resources were provided by the MRC-CBU, and office space for AT by the Centre for Speech, Language and the Brain. We thank Andrew Welchman for help and advice with stimuli design and equipment testing, and for comments and suggestions on an early draft of the manuscript. We would also like to thank Vassilis Pelekanos, Russell Thompson, Caroline Whiting, Elisabeth

Fonteneau, Anastasia Klimovich-Smith, Gary Chandler, Maarten van Casteren and Clare Cook for invaluable support and suggestions.

7. References

Brainard, D. H. (1997) The Psychophysics Toolbox, *Spatial Vision,* 10:433-436 doi: 10.1163/156856897X00357

Bone, R.A. and Sparrock, J.M.B. (1971). Comparison of macular pigment densities in the human eye. *Vis. Res.*11: 1057-1064. doi: 10.1016/0042-6989(71)90112-X

Cheng, M., Gao, X., Gao, S., Xu, D. (2001) Multiple color stimulus induced steady state visual evoked potentials. *Proc. IEEE EMBS*, 2:1012–1014. doi: 10.1109/IEMBS.2001.1020359

Conway B.R. (2001) Spatial structure of cone inputs to color cells in alert macaque primary visual cortex (V-1). *J Neurosci*. 21: 2768–83.

Conway, B. R., Chatterjee, S., Field, G. D., Horwitz, G. D., Johnson, E. N., Koida, K., and Mancuso, K. (2010) Advances in Color Science: From Retina to Behavior. *J. Neurosci*. 30:14955–14963 doi: 10.1523/JNEUROSCI.4348-10.2010

Dacey, D. M., Lee, B.B., Stafford, D.M., Smith, V.C., Pokorny, J. (1996) Horizontal cells of the primate retina: cone specificity without cone opponency. *Science*. 271: 656–8 doi: 10.1126/science.271.5249.656

Davis, M., Sigal, R. and Weyuker, E. J. (1994). *Computability, complexity, and languages: fundamentals of theoretical computer science*. Burlington, MA: Morgan Kaufmann Pub.

De Monasterio, F. M. & Gouras, P. (1975). Functional properties of ganglion cells of the rhesus monkey retina. J Physiol. 251, 167-195.

De Monasterio, F.M. and Schein, S.J. (1980) Protan-Like Spectral Sensitivity of Foveal Y Ganglion Cells of the Retina of Macaque Monkeys. *J. Physiol.* 299: 385-396

Derrington, M., Krauskopf, J., and Lennie, P. (1984) Chromatic Mechanisms in Lateral Geniculate Nucleus of Macaque. *J Physiol*. 357: 241-265 doi: 10.1113/jphysiol.1984.sp01549

Engel, S., Zhang, X and Wandell, B. (1997) Colour tuning in human visual cortex measured with functional magnetic resonance imaging. *Nature* 388: 68-71 doi: 10.1038/40398

Fairchild, M. D. (2013) *Color Appearance Models*, Third Edition. Oxford, England: Wiley

Fischl, B., Sereno, M. I., Tootell, R.B., Dale, A.M. (1999) High-resolution inter-subject averaging and a coordinate system for the cortical surface. *Hum Brain Mapp.* 8:272-284.

Gouras, P. (1968). Identification of cone mechanisms in monkey ganglion cells. J of Physiol 199, 533-547.

Grave de Peralta-Menendez, R., Gonzalez-Andino, S. L., and Lutkenhoner, B. (1996). Figures of merit to compare linear distributed inverse solutions. *Brain. Topogr.* 9:117–124. doi: 10.1007/BF01200711

Grave de Peralta-Menendez, R., and Gonzalez-Andino, S. L. (1998). A critical analysis of linear inverse solutions to the neuroelectromagnetic inverse problem. *IEEE Trans. Biomed.* Eng. 45, 440–8. doi: 10.1109/10.664200

Hadjikhani, N., Liu, A. K., Dale, A. M., Cavanagh, P., & Tootell, R. B. (1998). Retinotopy and color sensitivity in human visual cortical area V8. Nature Neuroscience, 1, 235–241

Hämäläinen, M.S., Ilmoniemi, R.J. (1994) Interpreting magnetic fields of the brain: minimum norm estimates. *Med Biol Eng Comput.* 32:35-42. doi: 10.1007/BF02512476

Hansen, T., and Gegenfurtner, K.R. (2009) Independence of color and luminance edges in natural scenes. *Vis Neurosci.* 26:35–49. doi:10.1017/S0952523808080796

Hauk, O., Wakeman D. G., and Henson, R. (2011). Comparison of noise-normalized minimum norm estimates for MEG analysis using multiple resolution metrics. *NeuroImage* 54, 1966-1974. doi: 10.1016/j.neuroimage.2010.09.053

Hering, E. (1878) *Zur Lehre vom Lichtsinn* Berlin: Springer

Herrmann, C.S. (2001). Human EEG responses to 1-100 Hz flicker: resonance phenomena in visual cortex and their potential correlation to cognitive phenomena. *Exp. Brain Res.* 137: 346–353. doi:10.1007/s002210100682

Hunt, R. W. G and Pointer, M. R. (1985) A colour appearance transform for the 1931 standard colorimetric observer. *Col Res Appl,* 10, 165-179 doi: 10.1002/col.5080100306

ISO/CIE (1999) ISO 10526:1999/CIE S005/E-1998: Standard Illuminants for Colorimetry. Vienna, Austria: ISO/CIE

ISO (2007) 11664-1:2007 Colorimetry -- Part 1: CIE standard colorimetric observers International Organization for Standardization, Geneva, Switzerland.

Ives, H. E. (1912). Studies in the photometry of lights of different colours. I. Spectral luminosity curves obtained by the equality of brightness photometer and flicker photometer under similar conditions. *Phil. Mag. Ser.* 6:149–188. doi: 10.1080/14786440708637317

693 Johnson, E. N., Hawken M. J. and Shapley R. (2001) The spatial transformation of
694 color in the primary visual cortex of the macaque monkey. *Nat. Neurosci.* 4, 409–
695 416 doi:10.1038/86061

696 Johnson, E. N., Hawken, M. J., Shapley, R. (2004) Cone inputs in macaque primary
697 visual cortex. *J Neurophysiol.* 91: 2501–14. doi:10.1152/jn.01043.2003.

698 Johnson, E.N., Hawken, M.J., Shapley, R. (2008) The orientation selectivity of color-
699 responsive neurons in macaque V1. *J Neurosci*. 28: 8096–106. doi:
700 10.1523/JNEUROSCI.1404-08.2008

701 Johnson, E.N., Mullen, K.T. (2016) Color in the Cortex. In: Kremers J., Baraas R.,
702 Marshall N. (eds) *Human Color Vision*. Springer: Cham: doi: 10.1007/978-3-319-
703 44978-4_7

704 Judd, D. B., (1951) Basic correlates of the visual stimulus *Handbook of Experimental*
705 *Psychology,* Stevens, S. S. (Ed), pp. 811-867. Oxford, England: Wiley

706 Kingdom, F.A. (2003) Color brings relief to human vision. *Nat Neurosci.* 6: 641–4.
707 doi:10.1038/nn1060

708 Kleiner, M., Brainard, D., Pelli, D. (2007) What's new in Psychtoolbox-3? *Perception*
709 36:14, doi:10.1177/03010066070360S101

710 Kommanapalli, D, Murray, I. J., Kremers, J., Parry, N. R. A. and McKeefry, D. J.
711 (2014) Temporal characteristics of L- and M-cone isolating steady-state
712 electroretinograms *J. Opt. Soc. Am.* A 31: A113-A120 doi:
713 10.1364/JOSAA.31.00A113

714 Kremers, J. and Link, B. (2008) Electroretinographic responses that may reflect
715 activity of parvo- and magnocellular post-receptoral visual pathways. *J Vis.* 8:1–14.
716 doi: 10.1167/8.15.11

717 Kremers, J., Rodrigues, A.R., Silveira, L.C.L., da Silva-Filho, M. (2010) Flicker
718 ERGs representing chromaticity and luminance signals. *Invest Ophthalmol Vis Sci.*
719 51:577–87 doi:10.1167/iovs.09-3899

720 Kunkel, T., Reinhard, E. (2009) A neurophysiology-inspired steady-state color
721 appearance model. *J Opt Soc Am A* 26:776-82. doi: 10.1364/JOSAA.26.000776

722 Kwong, K. K., Belliveau, J. W., Chesler, D. A., Goldberg, I. E., Weisskoff, R. M.,
723 Poncelet, B. P., et al. (1992). Dynamic magnetic resonance imaging of human brain
724 activity during primary sensory stimulation. *PNAS*, 89: 5675–5679 doi:
725 10.1073/pnas.89.12.5675

726 The Kymata Atlas; Cambridge University (2016) https://kymata.org/

727 Lalor, E.C., Pearlmutter, B.A., Reilly, R.B., McDarby, G., and Foxe, J.J. (2006) The
728 VESPA: a method for the rapid estimation of a visual evoked potential. *Neuroimage*
729 32:1549–1561. doi: 10.1016/j.neuroimage.2006.05.054

730 Li, C., Luo, M.R., Rigg, B., Hunt, R.W.G. (2002) CMC2000 Chromatic Adaptation
731 Transform: CMCCAT2000. *Col Res Appl*. 27:49-58 doi: 10.1002/col.10005

732 Lee, B.B., Silveira, L.C.L. (2016) Cone Opponency: An Efficient Way of
733 Transmitting Chromatic Information. In: Kremers J., Baraas R., Marshall N. (eds)
734 *Human Color Vision*. Springer: Cham. doi: 10.1007/978-3-319-44978-4_4

735 Leventhal, A.G., Thompson, K.G., Liu, D., Zhou, Y., Ault, S.J. (1995) Concomitant
736 sensitivity to orientation, direction, and color of cells in layers 2, 3, and 4 of monkey
737 striate cortex. *J Neurosci*. 15: 1808–18.

738 Levitt, J. B., Schumer, R. A., Sherman, S. M., Spear, P.D., and Movshon J. A. (2001)
739 Visual Response Properties of Neurons in the LGN of Normally Reared and Visually
740 Deprived Macaque Monkeys. *J Neurophys.* 85: 2111-2129. doi:
741 10.1152/jn.2001.85.5.211

742 Luo, M. R., and Hunt, R. W. G. (1998). Testing colour appearance models using
743 corresponding-colour and magnitude-estimation datasets. *Color Research &*
744 *Application 23*, 3, 147– 153. doi: 10.1002/(SICI)1520-6378(199806)23:3<147::AID-
745 COL6>3.0.CO;2-Q

746 Macleod, D. I. and Boynton, R. M. (1978) Chromaticity diagram showing cone
747 excitation by stimuli of equal luminance. *J Opt Soc Am.* 69: 1183-1186 doi:
748 10.1364/JOSA.69.001183

749 McKeefry, D.J. and Zeki, S. (1997) The position and topography of the human colour
750 centre as revealed by functional magnetic resonance imaging. *Brain*, 120**,** 2229–2242

751 Moroney, N., Fairchild, M. D., Hunt, R. W., Li, C., Luo, M. R., and Newman, T.
752 (2002). The CIECAM02 color appearance model. *10th Color and Imaging*
753 *Conference Final Program and Proceedings* (pp. 23-27). Society for Imaging Science
754 and Technology.

755 Nishifuji, S., Ohkado, H., Tanaka, S., 2006. Characteristics of alpha wave response to
756 flicker stimuli with color alternation. *Electronics and Communications in Japan, Part*
757 *3* (Translated from *Denshi Joho Tsushin Gakkai Ronbunshi*, 2005.) 89: 480-489.
758 doi: 10.1002/ecjc.20204

759 Ogawa, S., Tank, D., Menon, R., Ellermann, J., Kim, S., Merkle, H., et al (1992)
760 Intrinsic signal changes accompanying sensory stimulation: Functional brain mapping
761 with magnetic resonance imaging. *PNAS* 89:591–5955. Doi: 10.1073/pnas.89.13.5951

762 Parry, N. R. A., Murray, I. J., Panorgias, A., Mckeefry, D. J., Lee, B. B., Kremers, J.
763 (2012) Simultaneous chromatic and luminance human electroretinogram responses. *J*
764 *Physiol.* 150: 3141–3154 doi: 10.1113/jphysiol.2011.226951

765 Pelli, D. G. (1997) The VideoToolbox software for visual psychophysics:
766 Transforming numbers into movies, *Spat. Vis.* 10, 437-442. doi:
767 10.1163/156856897X00366

768 Regan, D. (1966). Some characteristics of average steady-state and transient
769 responses evoked by modulated light. *Electroencephalogr. Clin. Neurophysiol*. 20,
770 238–248. doi: 10.1016/0013-4694(66)90088-5

771 Ripamonti, C., Woo, W. L., Crowther, E., and Stockman, A. (2009) The S-cone
772 contribution to luminance depends on the M- and L-cone adaptation levels: Silent
773 surrounds? *J. Vision*, 9:10, 1–16, doi:10.1167/9.3.10.

774 Schmahmann, J. D., Doyon, J., Toga, A. W., Petrides, M., and Evans, A. C. (2000).
775 *MRI Atlas of the Human Cerebellum.* San Diego, CA: *Academic Press*.

776 Shapley, R., Hawken M. J. (2011) Color in the Cortex: single- and double-opponent
777 cells. *Vis. Res.* 51: 701–717 doi:10.1016/j.visres.2011.02.012

778 Smith, V.C., Lee, B. B., Pokorny, J., P. R. Martin, and A. Valberg, A. (1992)
779 Responses of macaque ganglion-cells to the relative phase of heterochromatically
780 modulated lights, *J. Physiol*. 458, 191-221. doi: 10.1113/jphysiol.1992.sp019413

781 Stockman, A., and Sharpe, L. T. (2000) Spectral sensitivities of the middle- and long-
782 wavelength sensitive cones derived from measurements in observers of known
783 genotype. *Vis. Res.*, 40, 1711-1737. doi: 10.1016/S0042-6989(00)00021-3

784 Stockman, A., Sharpe, L. T., and Fach, C. C. (1999) The spectral sensitivity of the
785 human short-wavelength cones. *Vis. Res.*, 39, 2901-2927. doi: 10.1016/S0042-
786 6989(98)00225-9

787 Taulu, S., Simola, J., Kajola, M. (2005) Applications of the signal space separation
788 method. IEEE T Signal Proces. 53:3359-3372. doi: 10.1109/TSP.2005.853302

789 Thorell, L.G., De Valois, R.L., Albrecht, D.G. (1984) Spatial mapping of monkey V1
790 cells with pure color and luminance stimuli. *Vision Res*. 24:751–69 doi:
791 10.1016/0042-6989(84)90216-5

792 Thwaites, A., Nimmo-Smith, I., Fonteneau, E., Patterson, R.D., Buttery, P., Marslen-
793 Wilson, W.D. (2015) Tracking cortical entrainment in neural activity: auditory
794 processes in human temporal cortex. *Front Comp Neurosci*.1-14 doi:
795 10.3389/fncom.2015.00005

796 Thwaites, A., Schlittenlacher, J., Nimmo-Smith, I., Marslen-Wilson W.D., Moore,
797 B.C.J. (2017) Tonotopic representation of loudness in the human cortex. *Hear. Res*.
798 344: 244-254 doi:10.1016/j.heares.2016.11.015

799 Thwaites, A., Glasberg, B.R., Nimmo-Smith, I., Marslen-Wilson W.D., Moore, B.C.J.
800 (2016) Representation of Instantaneous and Short-Term Loudness in the Human
801 Cortex. *Front. Neurosci*. 10: 183 doi:10.3389/fnins.2016.00183

802 Thwaites, A., Nimmo-Smith, I., Wieser, E., Soltan, A., Marslen-Wilson, W. D.
803 (2016b) *Measurement datasets 1-3.01 for the Kymata Atlas* [Dataset]. doi:
804 10.17863/CAM.1660

805 VanRullen, R. Macdonald, J.S.P. (2012) Perceptual Echoes at 10 Hz in the Human
806 Brain. *Cur Biol* 22:995–999 doi: 10.1016/j.cub.2012.03.050

807 Wachtler, T., Sejnowski, T.J., Albright, T.D. (2003) Representation of color stimuli in
808 awake macaque primary visual cortex. *Neuron*. 37: 681–91 doi: 10.1016/S0896-
809 6273(03)00035-7

810 Wade, A., Augath, M., Logothetis, N., Wandell, B. (2008). fMRI measurements of
811 color in macaque and human. *J Vis*, 8: 1–19, doi: 10.1167/8.10.6

812 Walraven, P. L., and Leebeek, H. J. (1964) Phase shift of alternating coloured stimuli
813 *Doc. Ophthalmol.* 18, 56–71. doi: 10.1007/BF00160563

814 Wandell, B. A. (1995) *Foundations of Vision*, Sunderland, MA: Sinauer Associates
815 Inc.

816 Wandell, B. A., Winawer, J. (2011) Imaging retinotopic maps in the human brain. *Vis*
817 *Res* 51:718–737 doi: 10.1016/j.visres.2010.08.004

818 Wiesel T, Hubel DH. (1966) Spatial and chromatic interactions in the lateral
819 geniculate body of the rhesus monkey. *J Neurophysiol.* 29:1115–56 doi:
820 10.1152/jn.1966.29.6.1115

821 Xu, X., Ichida, J., Shostak, Y., Bonds, A., and Casagrande, V. (2002). Are primate
822 lateral geniculate nucleus (LGN) cells really sensitive to orientation or direction? *Vis.*
823 *Neurosci.*, 19: 97-108. doi:10.1017/S0952523802191097

824

825